# Fatigue and Fracture Assessment for Reliability of Electronics Packaging

Soon-Bok Lee and Ilho Kim
*School of Mechanical, Aeronautics, and System Engineering, Korea Advanced Institute of Science & Technology, 373-1 Guseong-dong, Yuseong-ku, Daejeon, 305-701, Korea; e-mail: sblee@kaist.ac.kr; homepage: http://care.kaist.ac.kr*

**Abstract.** Modern electronics products move in the direction of complex, high density, high speed and also thinner and lighter for portability. Reliability of interconnection of electronics packaging has become critical issue. Major functions of electronic packaging are briefly discussed and failure mechanisms of electronic packaging are explained. Electronics packaging is subjected to mechanical vibration and thermal cyclic loads which lead to fatigue crack initiation, propagation and final fracture. A small sized electromagnetic type fatigue tester, micro-mechanical testing machine, and thermal fatigue testing apparatus were specially developed for reliability assessment of electronics packaging.
Long term reliability of surface mounted component packaging of under vibration induced high cycle fatigue was assessed with testing and finite element analysis. High cycle fatigue test was performed by the electromagnetic type testing machine. The time to failure was determined by measuring the changes in resistance. Using the micro-mechanical tester, isothermal low cycle fatigue of solder joints in packaging are performed and compared with finite element analysis to investigate the optimal shape of solder bumps in electronic packaging. Fatigue tests on various lead-free solder materials are discussed. Thermal fatigue tests of lead-contained and lead-free solder joints of electronic packaging were performed. Thermal fatigue results are compared with the mechanical fatigue data in terms of inelastic energy dissipation per cycle. It was found that mechanical load has longer fatigue life than thermal load at the same inelastic energy dissipation per cycle. Other advanced experimental methods for reliability assessment of microelectronic packaging are briefly discussed.

## 1. Introduction

Since modern electronics technology requires complex, high density, and high-speed devices, the use of surface mount components (SMC) has been increased. Due to the high degree of integration, high component density and the resulting high production cost of the surface mount technology, the modern advanced SMC assembly has imposed more stringent reliability requirements on packaging design. The ball grid array (BGA) package is a second level package, which is attached to a printed circuit board (PCB) through solder bumps to form a final second level assembly.
Moreover, the use of mobile devices has increased: cellular phones, personal data assistants (PDA), MP3 players, DVD players, portable multimedia players (PMP), and so on. In these mobile devices, the packages were exposed to the thermal and bending loads. The thermal loads were caused due to the thermal coefficient mismatch between different materials. Handing, key pressing and dropping induced bending loads on the solder joints. And, sometimes, mechanical and thermal load are combined together. These loads make the failure of solder joints. So the reliability tests need to be performed not only under thermal fatigue loading but also under mechanical fatigue loading.
Creep and the creep-fatigue interaction is the dominant mode of failure during thermal cycling. In that context, the creep and fatigue properties of lead-free solders have been studied extensively using bulk specimens. However, bulk materials usually have quite different microstructures from the actual solder-joint materials and, thereby, different mechanical properties, However, the mechanical properties of the solder joints are dependent on many factors such as the size, geometry, and microstructure of the solder joint under testing and service conditions. Thus in order to get a better understanding of the solder joint behavior, it is important to study real BGA solder joints attached to printed circuit boards.
Tin-lead eutectic alloys have been commonly used as solder material in microelectronic components. Environmental concerns on the toxicity of lead have resulted in legislation forbidding the use of lead in microelectronics products in the near future, prompting intensive searches for lead-free solder alloys.
In this study, to increase the electronic package reliability, various testing method are developed and reliability evaluation are conducted. Moreover, the design guide for solder shape and solder composition was introduced.

## 2. Solder optimization of solder bump

First, the effect of solder joint shape on the fatigue life is inspected (see Lee, et al., 2000). For the small size of solder joints, an accurate testing system was developed, which consists of testing machine part, a control and sensing part, and visual inspection part using a CCD camera (Figure 1). The testing machine

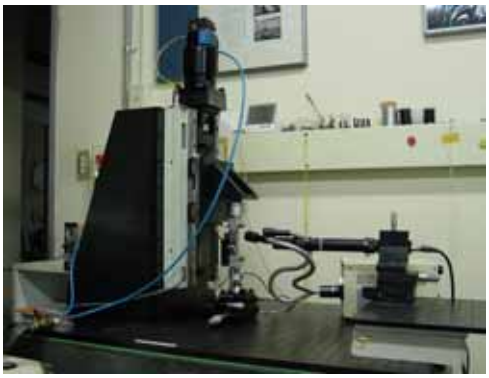

Figure 1. Micro-mechanical fatigue tester with high accurate load-cell, capacitance sensor and CCD camera.

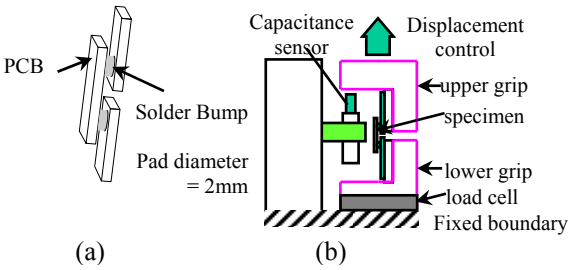


Figure 2. Configuration of the specimen and loading fixture; (a) The specimen having the two BGA type solder bumps: (b) Loading fixture of low cycle fatigue test

applied a load to the specimen via a step motor attached a ball screw driven rail table. The displacement of the specimen can be controlled with the resolution of 0.5um. The capacity of load cell is 500N and that signal can be acquired with the resolution of 2mV in the range of 10V. The PC controlled that system automatically and acquired all measured signals. The loading fixture for the specimen was designed to be suitable for pull shear and bending test of SMC/PCB assembly.

The specimens used in the experiments are three pieces of FR4 PCBs connected by two solder joints as shown in Figure 2(a). The thickness of the PCB is 1.6mm. Four different types of solder bumps are studied. The diameter of solder pad is 2mm. The solder paste used in the experiments was composed of 90% by weight of 63%Sn/37%Pb eutectic alloy balanced with rosin and solvent. To ensure good test specimens being assembled, the solder volume applied to each solder pad needs to be constant. For such a constant-volume control, solder pastes were printed to copper (Cu) pads by means of stencil printing.

In this approach, isothermal low cycle fatigue testing of solder bumps having the different shapes was performed with the machine that provides cyclic strain in the bumps at room temperature. The loading fixture for the specimen was designed to be suitable for fatigue load shown in Figure 2(b). The fatigue test was performed in a low cycle displacement controlled mode in which the joints were subjected to a fully reversed ramp cycle at the constant frequency of 1 Hz. The joints were deformed in shear with fixed displacement limits. The final fracture of the bumps could be detected using the resistance measurement. Through a visual inspection using a CCD camera, propagation of a crack could be observed after the crack is visible. But it is difficult to detect the instant of crack initiation using the both methods. So the crack initiation fatigue life was defined by 10% and 25% load drop.

In view of crack initiation fatigue life defined by 10% and 25% drop, it is observed the trend of increasing solder joint fatigue life with increasing height of bump. The correlation of crack initiation cycles $N_i$ versus maximum equivalent plastic strain is shown in Figure 3. The fatigue life curve of solder bumps with various shapes becomes straight lines. The equivalent plastic strain was obtained from the finite element analysis. Three dimensional finite element models are constructed to simulate the low cycle fatigue test of the specimens.

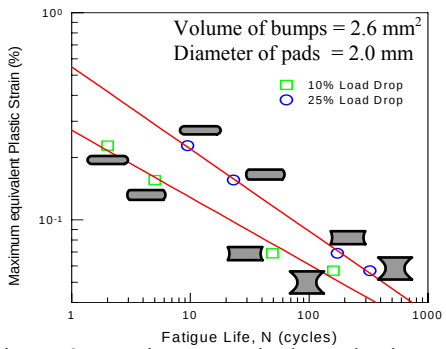


Figure 3. Maximum equivalent plastic strain versus fatigue life defined by 10% and 25% load drop

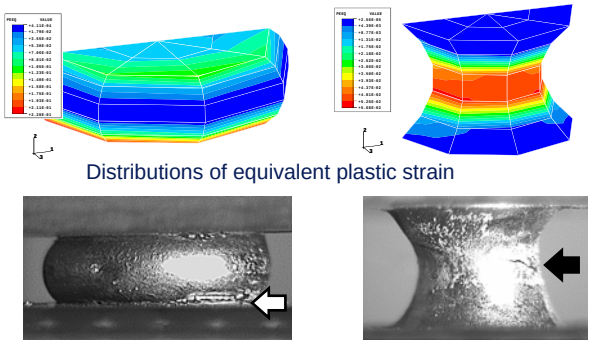


Figure 4. The prediction of crack location from the finite element analysis

The resulting equivalent plastic strain contours for the bumps with different shapes, an hourglass and a barrel shape, are shown in Figure 4. In barrel shape case, it can be seen that maximum equivalent plastic strain occurs near the interface between the pad and bump, while the hourglass-shaped bump has the maximum equivalent plastic strain at the center of the bumps. The results are consistent with the failure location as shown in Figure 4. Considering above result, maximum equivalent plastic strain was favored to be the governing parameter in fatigue life of a lead-tin eutectic BGA solder joint and we concluded that the optimal shape of lead-tin eutectic BGA solder joint is an hourglass shape.

## 3. Comparative study about compositions of lead-free solder and loading directions

A lot of lead-free solders are development for replacing the lead-contained solder. And in real operating condition, the loading direction is complex; it is not the pure tension and pure shear. In this section, the comparative study about composition of lead-free solder was performed using the micro-mechanical test. Further, the effects of loading direction are observed.

The chemical composition of six Sn-based solder alloys under investigation are presented in Table 1, and schematic diagram showing the lap-shear fatigue fixture is given in Figure 5. The solder balls of 0.76-mm diameter and 1.27-mm pitch were mounted to FR-4 printed circuit boards (PCBs), and the UBM structure consists of Cu/Ni/Au surface finishes with a pad-opening diameter of 0.594 mm. After solder reflow, the PCB/solder/PCB structure was mounted to a stainless-steel grip using an epoxy adhesive. The micromechanical test system used for the fatigue experiment has a servomotor attached to a ball screw-driven rail table to apply load to the specimen, and the displacement between grips was controlled to the accuracy of 50nm using a computer-controlled feedback system and a linear variable-differential transformer. Saw-tooth displacement waves with a frequency of 1/30 Hz were applied at room temperature under total displacement amplitudes of 10um, 12um, 15um, and 20um, with time lags between the displacement and load cycles caused by the time-dependent plasticity.

The load amplitude, the difference between the maximum and minimum loads, decreases with the load cycle, presumably, because of the propagation of fatigue cracks. Then, the number of load cycles that gave 50% load drop was defined as the fatigue life. Because the total displacement ($\Delta_T$) is the sum of the solder-ball displacement ($\Delta_S$) and the parasitic displacement ($\Delta_P$) coming from the loading systems (composed of a PCB, adhesives, and stainless-steel grips), $\Delta_P$ was measured using specimens without solder-ball attachment between the PCBs, and subsequently subtracted from $\Delta_T$ to give $\Delta_S$. Fatigue tests were performed after ten days at room temperature after solder reflow, which is known to stabilize the solder microstructure by age softening.

According to the load cycles, variations of the maximum force ($F_{max}$) in the force-displacement hysteresis are shown in Figure 6 for the six alloys. Note the following. (1) the magnitude of $F_{max}$ in the beginning of the load cycle decreases in the order of 7.5Bi, 2.5Bi, 1.5Cu, 0.75Cu, SnAg, and SnCu alloys. (2) Bi-containing alloys showed drastic decreases in $F_{max}$ after certain load cycles, implying fast fatigue-crack growth rate (da/dN) during the period. Load drop in all the other alloys were gradual.

The effects of Cu or Bi addition on the fatigue behavior of the Sn3.5Ag binary alloy are shown in Figure 7. The fatigue resistance increased slightly with Cu addition up to 0.75%, but tended to decrease with further additions. The increase of fatigue resistance from Sn3.5Ag to Sn3.5Ag0.75Cu results from the precipitation and solid-solution hardening with Cu addition. However, the dramatic increase of the $Cu_6Sn_5$ size from Sn3.5Ag0.75Cu to Sn3.5Ag1.5Cu had negative effects on fatigue resistance because the interface between $Cu_6Sn_5$ precipitates and the Sn matrix can act as the crack initiation sites. On the other hand, additions of Bi had deleterious effects on the fatigue life at all $\Delta$ values. (see Lee, et al., 2004)

Table 1. Chemical Composition of Solder Alloys

| Alloy | Sn | Ag | Bi | Cu |
|---|---|---|---|---|
| Sn-3.5Ag | 95.7 | 3.61 | | |
| Sn-3.5Ag-0.75Cu | 95.1 | 3.65 | | 0.75 |
| Sn-3.5Ag-1.5Cu | 94.6 | 3.49 | | 1.48 |
| Sn-3.5Ag-2.5Bi | 93.7 | 3.57 | 2.51 | |
| Sn-3.5Ag-7.5Bi | 88.5 | 3.63 | 7.62 | |
| Sn-0.7Cu | 99.4 | | | 0.57 |

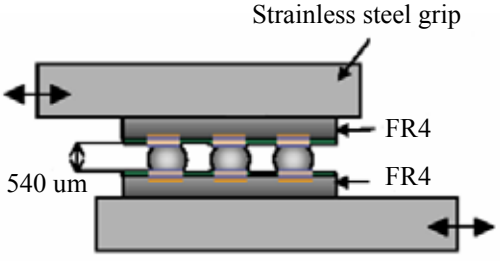

Figure 5. Fixture of lap-shear fatigue test

The mechanical fatigue test under mixed loading was performed in a displacement-controlled mode in which the specimen was subjected to a fully reversed triangle mixed load at a constant displacement rate of 2um/s. The applied displacement on the specimen was controlled to be constant until failure occurred and applied displacement amplitude was changed from 4 to 25um. To change the loading angle, several grips were prepared as shown in Figure. 8. An ac-type LVDT linear variable differential transformer was used to measure the relative displacement between grips. At least two specimens on each test condition were tested at various displacement amplitudes and loading angles. (see Park, et al., 2005)

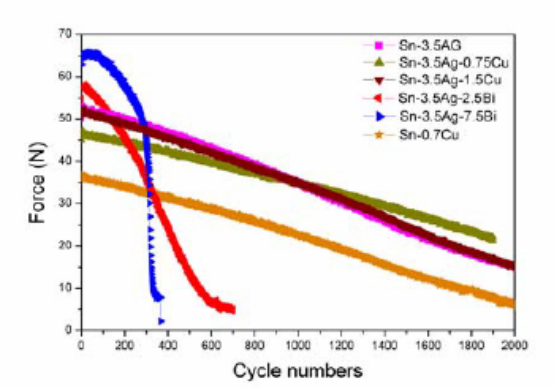


Figure 6. Variation of maximum force of the hysteresis with the cyclie number

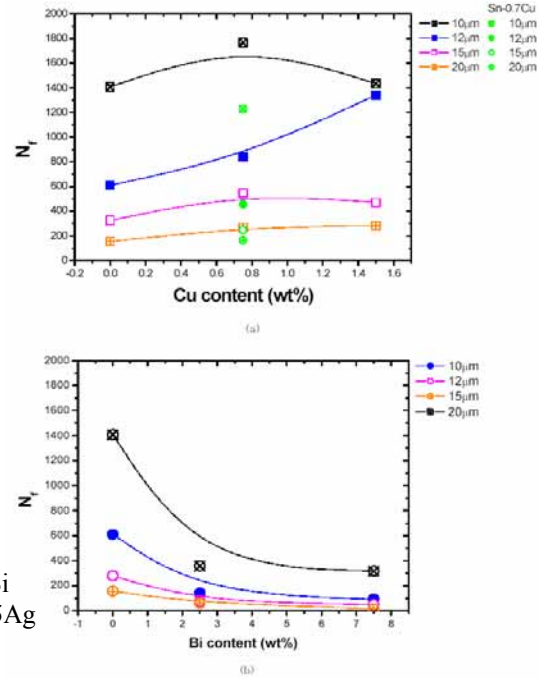


Figure 7. Effect of (a) Cu and (b) Bi addition on fatigue life of the Sn3.5Ag alloy under serveral $\Delta_T$ conditions.

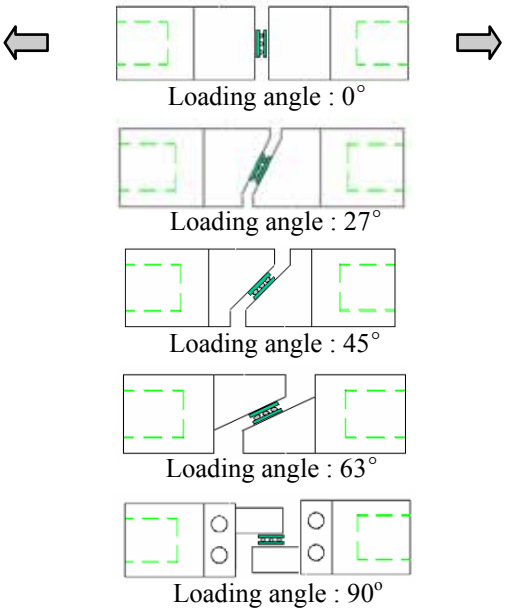


Figure 8. Test grip configuration. Loading angle is changed 0° to 90°.

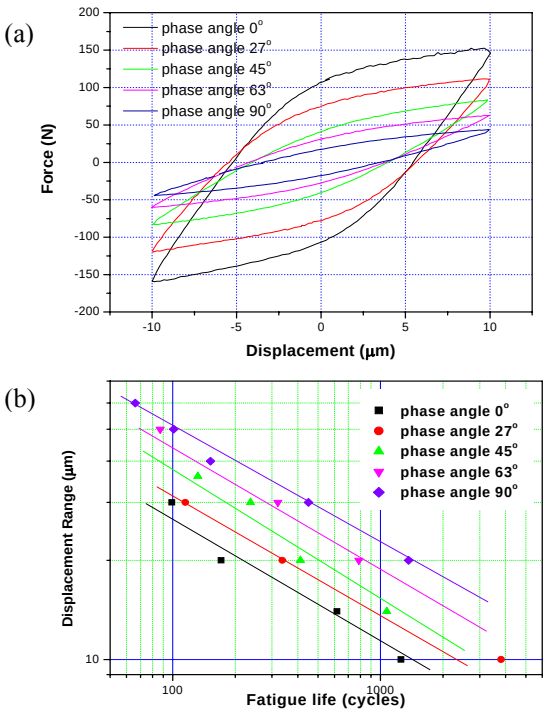


Figure 9. The loading angle effects : (a) Force versus displacement (b) Fatigue life versus displacement

The material behavior under ±10um constant displacement control is shown in Figure 9(a). Force displacement response is very different between the different loading angles. In the 0 deg loading angle, in pure tension compression loading case, the force displacement ratio is very stiff. Under the shear loading, the low modulus of the organic substrate enabled the solder joint to rotate on the substrate, which made the severe dependency on the loading angle in Figure 9(a). In this study, the load drop parameter was employed as failure criteria. The correlation of life cycles versus displacement stroke is shown in Figure 9(b). The fatigue life curves of solder bumps with various displacement ranges become straight lines within the same loading angle. There are apparent discrepancies between the loading angles.

## 4. Pseudo-power cycling test

Thermal fatigue tests were conducted with a pseudo-power cycling machine, which gives more realistic testing condition and higher efficiency of thermal fatigue test. Generally the power-cycling tests are required power (heating) chip and a precise control technique. It is exhausting work, so almost researchers do the chamber-cycling test. But the chamber-cycling test has many shortages. To overcome the power- and chamber-cycling test, the pseudo-power cycling test method was proposed (Park, 1998).In the pseudo-power cycling test, the heat transfer from the heater to package, so the package temperature goes up first and then the PCB temperature follow that. As a result, there exists a temperature gradient between the package and PCB like the power-cycling case. And the coolant takes heat out of the chip.
A schematic view and a real photograph of the pseudo-power cycling machine are presented at Figure 10(a) and 10(b). In order to achieve a uniform temperature distribution on the contact surface with the package, a shape of 'Test Base' and cooling channel's size, position and interval were designed through the finite element analysis. The temperatures of package and PCB, daisy chain's resistance were measured in real-time. The measured data was recorded on the PC. Moreover the PC makes the heater and coolant control signals automatically.

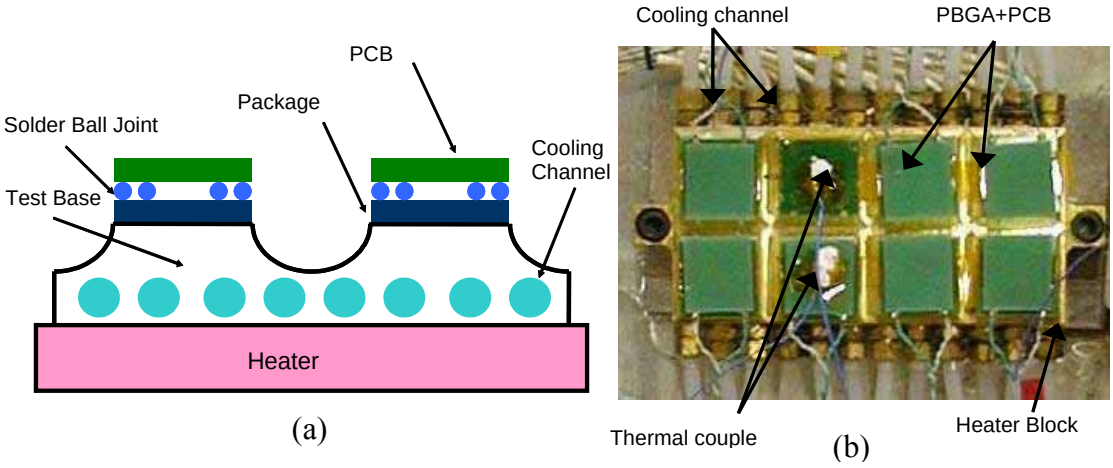


Figure 10. Schematic view; (a) and real real photograph (b) of pseudo-power cycling machine.

Tested specimen was shown as Figure 11. Two identical FR-4 PCBs of 2.0mm thickness were bonded by 36 solder joints, where 9 solder joints were laid on each corner. A lower PCB (white gray part at the Figure 11) which is used alike package is 40mm by 39mm and a upper PCB (dark gray part in the Figure 11) is 38mm by 34mm. The diameter of solder joints is 760μm and the pitch of solder joints is 1.27mm. For failure detection, daisy-chain is constituted.
The specimen has large size and small number of solder ball joints, it makes the package weaker than conventional package. Because the large size induces large thermal expansion mismatch between upper and lower PCB and small number of solder joints means that each solder joint is subjected to more stress under the same CTE mismatch. As a result, an acceleration test is possible using the this specimen.
The specimens are just placed on the top of the 'Test Base'. Thermal grease was applied to the contact surface of 'Test Base' to increase the conductivity between the 'Test Base' and package. It has enough viscosity to maintain the contact between package and the top surface of 'Test Base'. The testing conditions are listed on the Table 2.

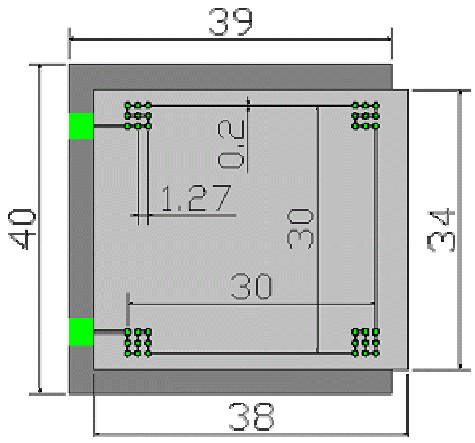

Figure 11. Specimen for pesudo-power cycling test.

Table 2. Testing conditions and time period

| 63Sn37Pb | 95.5Sn4.0Ag0.5Cu |
|---|---|
| 30~150 ºC | 30~150 ºC |
| 30~125 ºC | 30~130 ºC |
| 30~110 ºC | 30~110 ºC |
| 30~100 ºC | 30~100 ºC |
| 30~75 ºC | 30~90 ºC |
| | 30~70 ºC |

| | |
|---|---|
| Total cycle time | 7.5 min |
| Heating time | 3 min |
| Holding time | 3 min |
| Cooling time | 1.5 min |
| Cycles per day | 196 cycles |

Failure is defined when the resistance of the daisy chain exceeds 0.6Ω. Initial resistance of the daisy chain was 0.35Ω of room temperature, and 0.48Ω at high temperature region (150ºC). Higher temperature causes the thermal expansion on copper traces, so their length became longer and their area is reduced, which leads to increase the resistance of daisy chain. Figure 12 presents the changing trend of a daisy chain resistance. At early stage without any failures, the resistance profile followed the temperature profile of specimen as mentioned above. As the crack initiates and propagates, the resistance is increased and become unstable. When the crack is propagated thoroughly, the daisy chain is broken and the resistance goes to infinite. The resistance behavior showed irreversible process: once an unstable phenomenon started, it never become stable again. Hence, this failure criterion is thought to be reasonable. Pseudo-power cycling test results are arranged and summarized using Weibull distribution (see Kim, et al. 2004). The relationship between thermal fatigue life and ΔT is described in the Figure 13. There existed cross points between the lead-contained solder and the lead-free solders. In large ΔT regions lead-contained solder (63Sn37Pb) had a good fatigue resistance, but in small ΔT regions lead-free solder (95.5Sn4.0Ag0.5Cu) had a longer fatigue life. According to the result in Figure 13, the solder which exhibit a good reliability could be reversed defending on the testing conditions.

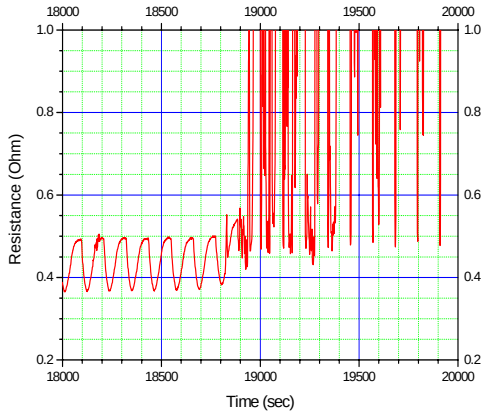

Figure 12. The changing trend of a daisy chain resistance.

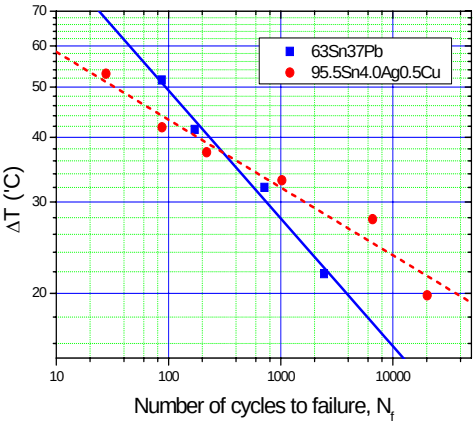

Figure 13. ΔT versus thermal fatigue life curve.

## 5. Cyclic bending test

In this study, 4-point bending test was conducted using micro-bending tester, which is developed for electronic package test. The testing machine applied a load to the specimen via an electro-magnetic coil guided through a linear busing. The 256PBGA is adopted for the bending test. Figure 14 shows the

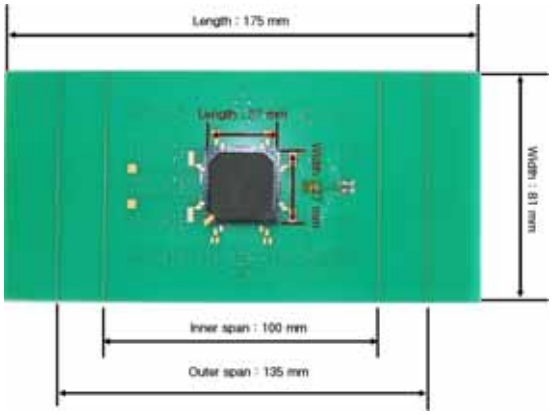


Figure 14. A specimen for four poins bending test

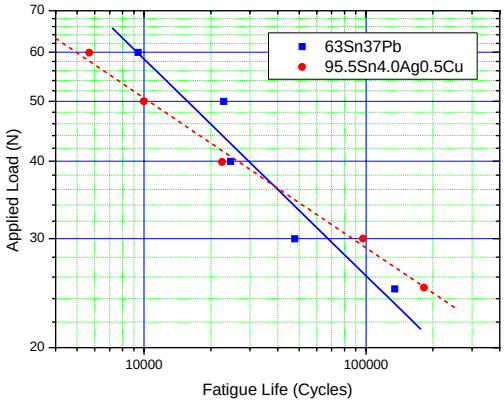


Figure 15. Applied load versus bending fatigue life curve

bending specimen. In the bending test, increased load could accelerate the test even if 256PBGA was used, because mechanical load could increase easily in comparison with thermal load.
Cyclic bending fatigue tests were performed using 1 Hz sinusoidal wave with various amplitudes ranging 25 to 60 N; the load increment size was 10 N. At each loading condition the test was repeated more than five times and the representative value for fatigue life was defined as their average value. The test results are described in the Figure 15. That result is similar to the pseudo-power cycling test. Under high load conditions, lead-contained solders have longer fatigue life. On the contrary, lead-free solder sustain more cyclic loads under small load conditions. According to Figures 13 and 15, it can conclude that lead-free solder has good fatigue resistance in small load and lead-contained solder could sustain large loads. (see Kim, et al. 2007)

## 6. Vibration-fatigue test

A small-sized vibration-fatigue testing machine was developed by utilizing an electromagnetic actuator to perform fatigue testing of electronic parts such as SMC assemblies. Figure 16 shows schematically a ceramic flat-pack surface mount assembly. It consists of four major parts: the package body, the leads, the solder joints and the printed circuit board. The SMC used in the test has 132 leads and a 0.64-mm pitch ceramic flat-pack. The dimensions of the packaging body are 24 mm x 24 mm x 2 mm. The spider gullwing shaped leads were bonded to the upper part of the package body by the thermo compression methods as shown in Figure 17.

Figure 16. Electromagnetic actuator and the load frame of the vibration-fatigue testing system

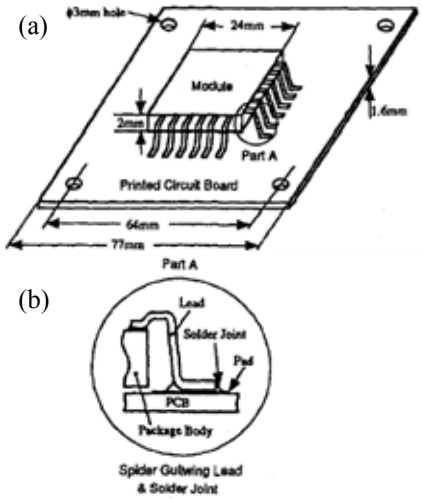


Figure 17. The specimen (a) PCB with a module attached in the center. (b) The detail of part A, showing a spder gullwing lead and solder joint

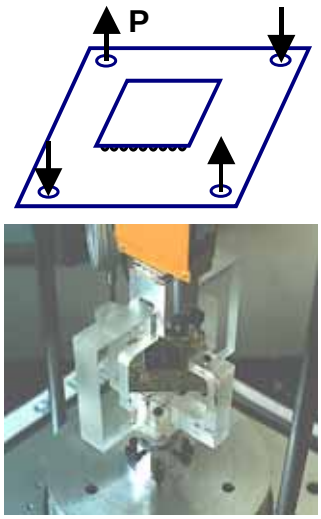


Figure 18. Electromagnetic actuator and the load frame of the vibration-fatigue testing system

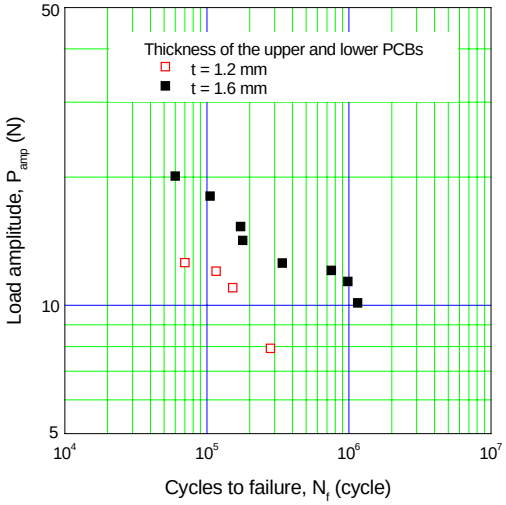


Figure 19. Electromagnetic actuator and the load frame of the vibration-fatigue testing system

The loading fixture for the specimen was designed to be suitable for torsion-fatigue loading shown in Figure 18. The torsion-loading fixture was made of acrylic plastic and fabricated in the top and bottom part. Each fixture has two screws to tighten the diagonally opposite corners of the plate for applying reversible loading. The top fixture is connected to the load cell of the loading frame, and the bottom fixture is mounted on the moving coil of the actuator. Hence the only bottom fixture is designed to move during the operation of the actuator. The applied load measured by the load cell needs to be divided by 2 because the force is distributed between two loading points.

The fatigue test was performed in a high-cycle force controlled mode in which the specimen was subjected to a fully reversed sinusoidal twisting load at the constant frequency of 40 Hz. The applied force on the specimen was measured by the load cell connected to the load frame, and the force was controlled to be constant until the failure occurred. The load amplitudes were between 2.5N and 10N. Six specimens were tested at various load amplitudes. Failure was defined in this study by the very rapid increase in daisy chain's resistance.

Figure 19 shows the fatigue test result indicating the load amplitude versus the number of cycles to failure. The applied loading is a fully reversed cyclic loading on the circuit card that varies from 10.26 N to 3.8 N, which creates a logarithmic distribution of the number of cycles from 23,600 to 1,399,200 as shown in Figure 19. There was no failure up to $10^7$ cycles in the case of 2.5 N. Each point on the curve represents a test specimen.

## 7. Conclusion

In this study, various testing method were developed and reliability evaluation was performed for solder joints.

(1) The effect of solder shape was investigated through the lap shear test. The fatigue life of solder joint is increased with increasing height of bump.

(2) The fatigue properties of six Sn-based, lead-free solders were investigated using lap shear specimens with ball grid array solder balls. The Sn3.5Ag, Sn0.7Cu, and Sn3.5AgCu alloys had similar fatigue resistance, but fatigue resistance degraded with the addition of Bi.

(3) The low cycle fatigue test of solder joints at room temperature under mixed-mode loading cases was performed. Force displacement responses are very different for different loading angles. Normal deformation affects significantly the fatigue life of the solder joints

(4) The pseudo power cycling method, developed to better simulate the real operating condition, was introduced. The lead-free solder has a stronger fatigue resistance than the lead-contained

solder under low temperature range. But, when the applied temperature range increased, the lead-contained solder has a longer fatigue life.

(5) The comparative study between lead-contained and lead-free solder under the cyclic bending test shows similar results with the pseudo power cycling test. At the high load region, the lead-contained solder has longer fatigue life. But in low load region, the lead-free solder has longer fatigue life.

(6) The vibration fatigue test for gull-wing leaded flat-pack was conducted. High-cycle fatigue curve corresponding to the $10^4$-$10^7$ cycle range of spider gull-wing leaded modules was generated by a torsion apparatus developed for circuit card systems.

## Acknowledgements

This work was supported by Ministry of Science and Technology in Korea through "Computer Aided Reliability Evaluation (CARE) for Electronic Packaging—National Research Laboratory (NRL) program" and "Development of Reliability Design Technique and Life Prediction Model for Electronic Components".

## References

Lee, S.-B., Park, T.-S. and Ham, S.-J. (2000). Experimental Techniques for Fatigue Reliability of BGA Solder Bumps in Electronic Packaging. *JSME International Journal Series* A43, 400-407.

Lee. K.O., Yu, J., Park, T.-S. and Lee, S.-B. (2004). Low-Cycle Fatigue Characteristics of Sn-Based Solder Joints, *Journal of Electronic Materials* 33, 249-257.

Park. T.-S., Lee, S.-B. (2005). Low Cycle Fatigue Testing of Ball Grid Array Solder Joints under Mixed-Mode Loading Conditions. *ASME transaction on Journal of Electronic Packaging* 127, 237-244.

Park, T.-S. (1998). *A Study for Reliability Assurance of Surface Mount Component Through Thermal Fatigue Testing*, Master's Thesis, MME98037, KAIST, Daejeon.

Kim, I., Park, T.-S., Yang, S.-Y. and Lee, S.-B. (2005). A Comparative Study of The Fatigue Behavior of SnAgCu and SnPb Solder Joints. *Key Engineering Materials* 297-300, 831-836.

Kim, I. and Lee, S.-B. (2007). Fatigue Life Evaluation of Lead-free Solder under Thermal and Mechanical Loads. *57th Electronic Components and Technology Conference*, 95-104.

Ham, S.-J. and Lee, S.-B. (1996). Experimental Study for Reliability of Electronic Packaging under Vibration, *Experimental Mechanics* 36, 39-344.